Acta Mechanica 121, 191–213 (1997)

ACTA MECHANICA

Nodal sensitivities as error estimates in computational mechanics

G. H. Paulino, F. Shi, S. Mukherjee, Ithaca, and **P. Ramesh,** Webster, New York

(Received June 19, 1995; revised November 27, 1995)

Summary. This paper proposes the use of special sensitivities, called nodal sensitivities, as error indicators and estimators for numerical analysis in mechanics. Nodal sensitivities are defined as rates of change of response quantities with respect to nodal positions. Direct analytical differentiation is used to obtain the sensitivities, and the infinitesimal perturbations of the nodes are forced to lie along the elements. The idea proposed here can be used in conjunction with general purpose computational methods such as the Finite Element Method (FEM), the Boundary Element Method (BEM) or the Finite Difference Method (FDM); however, the BEM is the method of choice in this paper. The performance of the error indicators is evaluated through two numerical examples in linear elasticity.

1 Introduction

This paper proposes the use of *special sensitivities,* called *nodal sensitivities,* as error indicators or estimators in numerical analysis with methods such as the Boundary Element Method (BEM), the Finite Element Method (FEM) or the Finite Difference Method (FDM). *Nodal sensitivities are defined here as rates of change of response quantities (such as displacement, traction, stress or temperature) with respect to nodal positions (geometrical variables).* The infinitesimal nodal perturbations are restricted such that the perturbed position is also on the element. Two schemes for nodal perturbation, Lagrangian and Eulerian, are described later in this paper. The Eulerian scheme, adopted in this work, leaves the shape of the element unchanged. Thus, sensitivities obtained by this approach are strictly due to a "mesh perturbation" without any change in the shape of the body.

This proposal of using nodal sensitivities as error indicators, although heuristic in nature, has several appealing features. The first is that when a numerical solution coincides with the exact one, it is, of course, no longer mesh sensitive. The second is a calculation of "interpolation error", which shows that, for the case considered herein, the nodal sensitivity of the solution is equal to the slope of the "interpolation error" with respect to the nodal perturbation ε. Of course, one is typically interested in "approximation errors" (rather than "interpolation errors") in BEM or FEM computations. However, the simple calculation involving "interpolation errors" serves as a logical motivation for the use of nodal sensitivities as error indicators.

A unique feature of the work presented in this paper is that nodal sensitivities are obtained by analytical differentiation with respect to simultaneous perturbations of groups of nodes. This approach is very efficient and establishes a natural linkage between geometric modeling and engineering analysis. It is felt that further use of the techniques presented in this paper could be a significant contribution towards a reliable and automated environment in computational mechanics, in the sense described by, for example, Tworzydlo and Oden [1], Finnigan et al. [2],

and Shephard and Finnigan [3]. Further discussions on error estimation techniques in computational mechanics can be found in Reference [4].

The remainder of this paper is organized as follows. Initially, a brief literature survey and comments on previous related work are presented. Next, Eulerian and Lagrangian nodal perturbation schemes are discussed. Afterwards, a motivation is given for using nodal sensitivities as error indicators in computational mechanics. By means of a simple and enlightening example, the nodal sensitivity is related to the "interpolation error". The next Section is devoted to the actual method for obtaining error indicators. The standard BEM and the Derivative BEM (DBEM) are compared, and the use of the latter method is justified. Then, the special sensitivity formulation of the DBEM is presented in detail. A general procedure for obtaining design velocities is outlined and exemplified for two special cases. Next, the error indicators are presented. In order to validate the method presented here, two numerical examples, for which there exist available analytical solutions, are given. Finally, conclusions are inferred and extensions of this work are pointed out.

2 Related work

Several papers are important to the present work. Some of these papers are listed and commented on below. Kelly et al. [5] have presented *a posteriori* estimates of the solution error caused by discretization in the finite element, finite difference and boundary element methods. They have presented a theory that guarantees upper and lower bound estimates of the discretization error in numerical solutions of elliptic boundary value problems. Two examples in potential theory have been presented and applied to the FEM, BEM and FDM. Mitra et al. [6] recognized the importance of both geometric as well as functional discretization for the accuracy of BEM solutions. They have presented a two-step spline assisted grid optimization scheme for the BEM. Lean [7] has presented an adaptive mesh refinement scheme for solving magnetostatics problems by the BEM. He has pointed out that Φ, $\partial\Phi/\partial\boldsymbol{n}$, $D\Phi$ and $D(\partial\Phi/\partial\boldsymbol{n})$ can be used as possible criteria for mesh refinement in the solution of the linear problem. The variables Φ and $\partial\Phi/\partial\boldsymbol{n}$ denote potential and boundary flux, respectively, D is the tangential derivative operator ($D \equiv \partial/\partial t$), and $\boldsymbol{n}$ and $\boldsymbol{t}$ refer to the normal and tangential directions on the boundary of a two-dimensional (2-D) body. Recently, Paulino [4] and Paulino et al. [8] have applied the concept of directional derivatives of a Boundary Integral Equation (BIE) in order to develop an error estimation technique intrinsic to the BEM. This class of error estimates has been called "hypersingular residuals" because it is based on the residual of a hypersingular BIE. Bugeda and Oliver [9] have presented a methodology for 2-D shape optimization problems analyzed by the FEM. The boundary of the body is parameterized with B-splines. They perform sensitivity analyses of several response variables which include nodal coordinates (mesh sensitivity analysis) and the former Zienkiewicz and Zhu [10] error estimator[1]. *Note that, in the present work, the sensitivities themselves are used as the error indicators.* Sussman and Bathe [13] have investigated the gradient of the total potential energy (II) with respect to nodal point-coordinates in the FEM. They have used these gradients to solve a simple example involving fracture mechanics and mesh optimization. In this particular example, the stress intensity factors of a Mode I crack are accurately determined using a finite element mesh which was improved upon using mesh optimization.

[1] In 1992, Zienkiewicz and Zhu published two consecutive papers [11], [12] which superseded their earlier work [10].

Recent work by Guiggiani [14], Guiggiani and Lombardi [15] (which is a follow-up paper of Reference [14]) and Henneberger et al. [16] are closely related to the present work. Guiggiani [14] has determined how a BEM solution in linear elasticity changes due to *finite perturbations* in the positions of collocation points. He perturbs all the boundary collocation points, that are situated interior to boundary elements, together. He has carried out numerical experiments with different magnitudes of these finite perturbations. His method is based on the fact that, specifically in the collocation BEM, there exists the possibility of obtaining more than one numerical solution from a given boundary element mesh. Error indicators are obtained by comparing two BEM solutions which refer to the same boundary nodes, but with partly different sets of collocation points. This work was revisited by Guiggiani and Lombardi [15]. They added h-hierarchical shape functions and changed the norm for displacements in the error indicator. Henneberger et al. [16] have also calculated sensitivities of a response variable with respect to nodal positions – this time in the context of the FEM applied to electromagnetic problems. The response variable in their work is the total magnetic energy. The energy perturbation of the nodal position is used as the refinement indicator of the mesh generator. It is not clear from their paper exactly how the derivatives are evaluated, e.g. $\partial A_j/\partial x_i$, $\partial|G|/\partial x_i$, etc. In these quantities, $\boldsymbol{A}$ is the vector potential, $|G|$ is a certain Jacobian and x_i is the x coordinate of node i. Also, Henneberger et al. [16] calculate sensitivities with respect to each node separately, a procedure that can become extremely computer expensive, especially for three-dimensional (3-D) problems.

In the present paper, sensitivities of response variables (such as tractions and generalized displacements), with respect to the positions of middle nodes of quadratic boundary elements, are calculated by direct analytic differentiation of the governing BEM equations of a problem. This Direct Differentiation Approach (DDA) is accepted as being more accurate, in general, than the Finite Difference Approach (FDA) for calculation of sensitivities (see, for example, Chapter 7 of the book by Haftka and Gürdal [17]). The FDA uses the finite difference of two neighboring solutions – one with a "reference" and the other with a "perturbed" set of design variables (here the position of certain boundary nodes) to calculate sensitivities. Also, the present work proposes an efficient analytical procedure for calculating sensitivities of response variables with respect to the positions of all the mid-side nodes of all the boundary elements together. It is worth restating that the idea of using nodal sensitivities as error indicators is generally applicable to a variety of numerical methods (e.g. BEM, FEM, and FDM); although the details have been carried out here for the BEM only. Moreover, the present method can be directly used with existing codes since the sensitivity solution is obtained in a post-processing stage, i.e. after the solution of the boundary value problem. This is not the case with the work by Guiggiani [14], which is specific to the BEM, and requires modification of the actual BEM implementation and special treatment of singular integrals.

3 Nodal perturbation schemes

There are various possibilities for perturbing nodes in a mesh. The nodal perturbation schemes are classified here in two groups: Lagrangian and Eulerian [4]. These schemes are illustrated by means of Fig. 1, which shows the perturbation of the middle node of a quadratic boundary element.

3.1 Lagrangian

Figure 1a shows the original and perturbed nodal configuration schemes. The middle node is perturbed along the physical boundary of the body. Its intrinsic coordinate, however, remains at

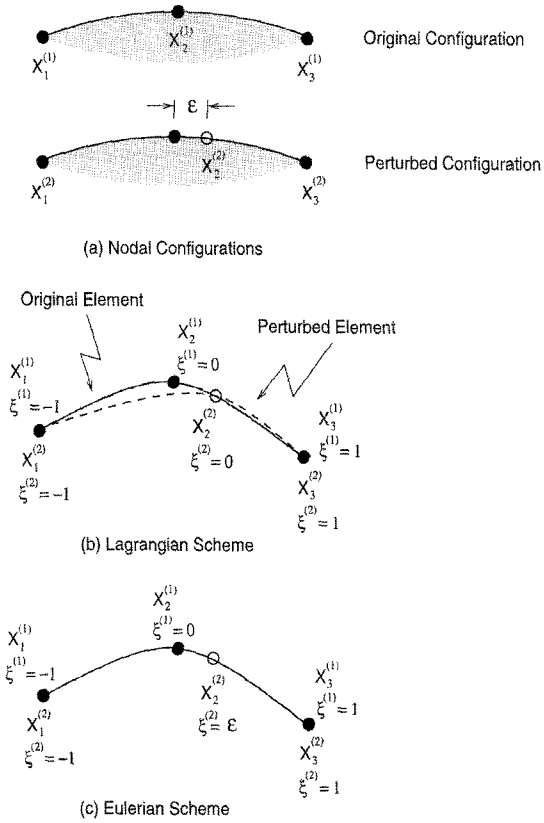

Fig. 1. Schemes for perturbing the middle node of a quadratic boundary element; $X_i^{(j)}$ denotes the Cartesian coordinate of node i in the configuration (j), where $j = 1$ refers to the original configuration and $j = 2$ refers to the perturbed configuration

the location $\xi = 0$, as shown in Fig. 1 b. Consequently, the shape of the quadratic boundary element is altered and the sensitivity of a length element ds with respected to the nodal perturbation (i.e. $\overset{*}{ds}$)[2] is *not* zero. Using the BEM for potential problems, Shi et al. [18] have employed the DDA to compute sensitivities of response variables (potential and flux), with respect to the positions of the intermediate nodes of pairs of linear boundary elements. All the pairs of linear boundary elements in the mesh are perturbed simultaneously.

3.2 Eulerian

Figure 1 c shows the Eulerian scheme for perturbing the middle node of a quadratic boundary element. Now the middle node is perturbed along the quadratic boundary element. The intrinsic coordinate of the middle node is perturbed from $\xi = 0$ to $\xi = \varepsilon$ (see Section 4 and Appendix A), as shown in Fig. 1 c. Consequently, the shape of the quadratic boundary element is *not* altered and the sensitivity of a length element ds with respect to the nodal perturbation (i.e. $\overset{*}{ds}$)[2] is zero. In this work, the Eulerian nodal perturbation scheme is adopted. The BEM for elasticity problems is considered, and the DDA is used to compute sensitivities of response variables (generalized displacements and tractions), with respect to the positions of the middle nodes of quadratic elements.

[2] The quantity $\overset{*}{ds}$ is explained in detail later in this paper.

4 Motivation for using nodal sensitivities as error estimates

This Section provides a motivation for using nodal sensitivities as error estimates in computational mechanics. In particular, it attempts to relate the nodal sensitivity of a generic function to the error by means of simple *interpolation* concepts. Thus, the reasoning below should be understood just as a *motivation* to the present work because numerical methods, such as BEM and FEM, essentially involve *approximation*, which is not considered in this Section.

By definition, the local error

$$e_\phi = \phi_e - \phi_a \tag{1}$$

is a measure of the difference between the exact (ϕ_e) and an approximate (ϕ_a) solution to a response quantity ϕ. Figure 2 is used to illustrate the present derivations. Note that, in a numerical method, the calculated nodal values have some discretization error, which is neglected in this figure. From the definition in Eq. (1),

$$\phi_e(\xi) = \phi_a(\xi) + e_\phi(\xi) \tag{2}$$

where $\phi_a(\xi)$ is a quadratic interpolation of $\phi_e(\xi)$ at $\xi = -1, 0, 1$, and by definition, $e_\phi(-1) = e_\phi(0) = e_\phi(1) = 0$. Thus, $\phi_a(\xi)$ is a quadratic function which can be expressed as

$$\phi_a(\xi) = \phi_A M_1(\xi) + \phi_B M_2(\xi) + \phi_C M_3(\xi), \tag{3}$$

where $\phi_A = \phi_e(-1)$, $\phi_B = \phi_e(0)$, $\phi_C = \phi_e(1)$, and the standard shape functions $M_i(\xi)$, $i = 1, 2, 3$, are

$$M_1(\xi) = \frac{\xi(\xi - 1)}{2},$$

$$M_2(\xi) = (1 - \xi)(1 + \xi), \tag{4}$$

$$M_3(\xi) = \frac{\xi(\xi + 1)}{2}.$$

Now suppose that one seeks an alternative expression for $\phi_a(\xi)$ in terms of its values at the same end-points A and C, but at a different interior point $\tilde{B}$ located at $\xi = \varepsilon$ (see Fig. 2). Considering Eq. (3) with $\xi = \varepsilon$,

$$\phi_a(\varepsilon) = \phi_A M_1(\varepsilon) + \phi_B M_2(\varepsilon) + \phi_C M_3(\varepsilon) \tag{5}$$

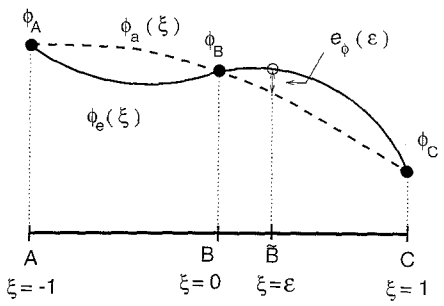

Fig. 2. $\phi_a(\xi)$ is a quadratic interpolation of $\phi_e(\xi)$. Note that both functions have the same values at A, B and C

and solving for ϕ_B, one obtains

$$\phi_B = \frac{1}{M_2(\varepsilon)} [\phi_a(\varepsilon) - \phi_A M_1(\varepsilon) - \phi_C M_3(\varepsilon)]. \tag{6}$$

Substitution of Eq. (6) into Eq. (3) gives

$$\phi_a(\xi, \varepsilon) = \phi_A \left[M_1(\xi) - \frac{M_1(\varepsilon)}{M_2(\varepsilon)} M_2(\xi) \right] + \phi_C \left[M_3(\xi) - \frac{M_3(\varepsilon)}{M_2(\varepsilon)} M_2(\xi) \right] + \phi_a(\varepsilon) \frac{M_2(\xi)}{M_2(\varepsilon)}. \tag{7}$$

Define a new function $\phi_{ea}(\xi, \varepsilon)$ which has the same form as ϕ_a in Eq. (7), but with $\phi_a(\varepsilon)$ replaced by the exact value $\phi_e(\varepsilon)$, given by Eq. (2). Simplifying the resulting expression by means of Eqs. (6) and (3), one obtains

$$\phi_{ea}(\xi, \varepsilon) = \phi_a(\xi) + \frac{e_\phi(\varepsilon) M_2(\xi)}{M_2(\varepsilon)}. \tag{8}$$

Note that $\phi_{ea}(\xi, \varepsilon)$ is simply a quadratic interpolation of $\phi_e(\xi)$ at $\xi = -1, \varepsilon, 1$, and by definition, $e_\phi(-1) = e_\phi(\varepsilon) = e_\phi(1) = 0$.

The sensitivity of $\phi_{ea}(\xi, \varepsilon)$ with respect to the position of the interior interpolation point $\tilde{B}$ is

$$\overset{*}{\phi}_{ea}(\xi, \varepsilon) = \frac{\partial \phi_{ea}(\xi, \varepsilon)}{\partial \varepsilon} \tag{9}$$

which can be readily obtained from Eq. (8),

$$\overset{*}{\phi}_{ea}(\xi, \varepsilon) = \left\{ \frac{e_\phi'(\varepsilon)}{M_2(\varepsilon)} - \frac{\varepsilon_\phi(\varepsilon) M_2'(\varepsilon)}{[M_2(\varepsilon)]^2} \right\} M_2(\xi), \tag{10}$$

where the fact that $\overset{*}{\xi} = 0$ has been used above. Finally, the sensitivity at the mid-point B is obtained by setting $\varepsilon = 0$ and $\xi = 0$ in Eq. (10), and thus

$$\overset{*}{\phi}_{ea}(0, 0) = e_\phi'(0) \tag{11}$$

since $M_2(0) = 1$ and $M_2'(0) = 0$. *Equation (11) shows that the nodal sensitivities of ϕ_{ea} at the mid-point B are equal to the slope of the (interpolation) error function at that point.*

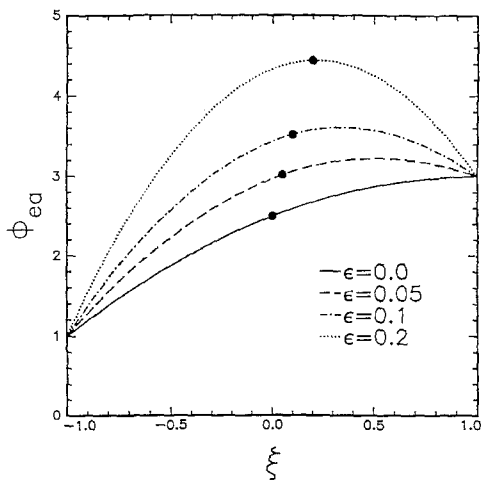

Fig. 3. $\phi_{ea}(\xi, \varepsilon)$ as function of ξ for different values of ε. Here $\phi_A = 1.0$, $\phi_B = 2.5$, $\phi_C = 3.0$ and $e(\xi) = 3 \sin(\pi\xi)$. The bullets correspond to $\phi_{\tilde{B}}$ for $\tilde{B}$ located at $\xi = 0.0, 0.05, 0.1$, and 0.2

4.1 A simple example

A simple example, which illustrates the motivation for using nodal sensitivities as error estimates, is given in Fig. 3. The error function has been arbitrarily chosen as $e_\phi(\xi) = \alpha \sin(\pi\xi)$, where $\alpha = 3$ in Fig. 3.

4.2 Comments

Note that ϕ_{ea} is the general quadratic interpolation of ϕ_e at $\xi = -1, \varepsilon, 1$. Indeed, ϕ_a is a particular case of ϕ_{ea}. This can be immediately verified by setting $\varepsilon = 0$ and using $e_\phi(0) = 0$ in Eq. (8) (see also Fig. 3) to obtain

$$\phi_{ea}(\xi, \varepsilon)|_{\varepsilon=0} = \phi_a(\xi). \tag{12}$$

The above discussion motivates the use of *nodal sensitivities* as *error indicators* in numerical methods. Although a quadratic interpolation has been assumed, this discussion can be readily extended to higher order polynomials (also see Appendix A). Moreover, a complete discussion would require a rigorous analysis of a solution obtained from a numerical technique such as the BEM or FEM. This analysis is not carried out here.

5 Eulerian framework for sensitivity and error analyses

The main idea in this work is that *if a numerical solution matches the exact solution of a boundary value problem, then it is not sensitive to perturbation of internal nodes within elements. Therefore, the sensitivities of the numerical solution with respect to the nodal perturbations are used here as error indicators.* Consider the solution of a boundary value problem where ϕ is a generic variable. Then

$$\overset{*}{\phi} = \lim_{\varepsilon \to 0} \frac{\phi|_{\text{mesh1}} - \phi|_{\text{mesh2}}}{\varepsilon} \tag{13}$$

in which $\phi|_{\text{mesh1}}$ and $\phi|_{\text{mesh2}}$ represent the specific values of the response variable corresponding to the adopted discretizations for two mesh configurations (mesh 1 and mesh 2, respectively) for exactly the same problem. If ϕ can be exactly represented by the adopted basis functions, then, clearly $\overset{*}{\phi} = 0$.

Here, the middle node of each quadratic boundary element is perturbed, in Eulerian sense, from $\xi = 0$ to $\xi = \varepsilon$ (see Fig. 1 c) and the same set of interpolation functions is used for both cases. However, for the perturbed mesh, these functions are constructed in terms of the values at $\xi = -1, \varepsilon, 1$. This is expressed by Eq. (7), which can be rewritten as (see Fig. 2)

$$\phi(\xi, \varepsilon) = \phi_A \tilde{M}_1(\xi, \varepsilon) + \phi_{\tilde{B}} \tilde{M}_2(\xi, \varepsilon) + \phi_C \tilde{M}_3(\xi, \varepsilon) \tag{14}$$

with

$$\begin{aligned}
\tilde{M}_1(\xi, \varepsilon) &= M_1(\xi) - \frac{M_1(\varepsilon)}{M_2(\varepsilon)} M_2(\xi), \\
\tilde{M}_2(\xi, \varepsilon) &= \frac{M_2(\xi)}{M_2(\varepsilon)}, \\
\tilde{M}_3(\xi, \varepsilon) &= M_3(\xi) - \frac{M_3(\varepsilon)}{M_2(\varepsilon)} M_2(\xi).
\end{aligned} \tag{15}$$

For the differential element ds of the length parameter s

$$\overset{*}{ds} = 0 \tag{16}$$

because ds is not a function of ξ or ε. Neither the shape of the body nor the element density changes (i.e. no distortion or stretching). However, to be consistent, $\overset{*}{\phi}$ must include contributions from $\overset{\#}{M}_i$. From Eq. (14),

$$\begin{aligned}\overset{*}{\phi}(\xi) = \lim_{\varepsilon \to 0} [&\overset{*}{\phi}_A \tilde{M}_1(\xi, \varepsilon) + \overset{*}{\phi}_{\tilde{B}} \tilde{M}_2(\xi, \varepsilon) + \overset{*}{\phi}_C \tilde{M}_3(\xi, \varepsilon) \\ &+ \phi_A \overset{\#}{\tilde{M}}_1(\xi, \varepsilon) + \phi_{\tilde{B}} \overset{\#}{\tilde{M}}_2(\xi, \varepsilon) + \phi_C \overset{\#}{\tilde{M}}_3(\xi, \varepsilon)].\end{aligned} \tag{17}$$

It can be easily shown that (see Fig. 1c)

$$\begin{aligned}&\lim_{\varepsilon \to 0} \overset{\#}{\tilde{M}}_1(\xi, \varepsilon) = \frac{1}{2} M_2(\xi), \\ &\lim_{\varepsilon \to 0} \overset{\#}{\tilde{M}}_2(\xi, \varepsilon) = 0, \\ &\lim_{\varepsilon \to 0} \overset{\#}{\tilde{M}}_3(\xi, \varepsilon) = -\frac{1}{2} M_2(\xi).\end{aligned} \tag{18}$$

Considering the limit $\varepsilon \to 0$ and substituting Eqs. (18) in Eq. (17), one obtains

$$\overset{*}{\phi}(\xi) = \overset{*}{\phi}_A M_1(\xi) + \overset{*}{\phi}_B M_2(\xi) + \overset{*}{\phi}_C M_3(\xi) + \frac{1}{2} (\phi_A - \phi_C) M_2(\xi). \tag{19}$$

where the last term arises due to the sensitivity of the shape functions. Note that in this case $\tilde{B} \equiv B$. Equation (19) is used later in the numerical discretization.

6 The error estimation method

The proposed error estimation method, in conjunction with the Derivative Boundary Element Method (DBEM), is presented in this Section. Of course, the idea of using nodal sensitivities as error indicators can be applied together with other computational techniques such as the FEM.

6.1 Boundary element formulations

The standard direct BEM formulation for linear elasticity [19], in the absence of body forces, can be written as

$$C_{ij}(P)\, u_i(P) = \int_{\partial B} [U_{ij}(P, Q)\, \tau_i(Q) - T_{ij}(P, Q)\, u_i(Q)]\, ds(Q) \tag{20}$$

where $\boldsymbol{u}$ and $\boldsymbol{\tau}$ are the displacement and traction vectors, respectively, $\boldsymbol{C}$ is the corner tensor, $\boldsymbol{U}$ and $\boldsymbol{T}$ are the usual Kelvin kernels (see Appendix B), and ds denotes a differential length element in 2-D, or a differential surface element in 3-D problems. The upper case letters P and Q denote the source and field points, respectively, on the boundary ∂B of a body B. The first integral on the Right-Hand-Side (RHS) of Eq. (20) is weakly singular and the second integral is strongly singular. This last integral can be evaluated by direct [20], [21] or indirect [20] approaches. Note that the functional form of Eq. (20) holds for both 2-D and 3-D problems.

Ghosh et al. [22] and Ghosh and Mukherjee [23] have proposed a derivative BEM (DBEM) where the tractions are still retained as primary boundary variables, but the displacements

are not. Instead, the other primary boundary variables are the tangential derivative of the boundary displacements $\partial u_i/\partial s$ ($i = 1, 2$) for 2-D problems [22] or the displacement gradients $u_{i,j}(i, j = 1, 2, 3)$ for 3-D problems [23].

For a simply-connected 2-D region B with boundary ∂B, the DBEM formulation is of the form

$$\int_{\partial B} [U_{ij}(P, Q)\, \tau_i(Q) - W_{ij}(P, Q)\, \Delta_i(Q)]\, ds(Q) = 0 \tag{21}$$

where $i, = 1, 2; j = 1, 2$, and, as explained before, $\Delta_i = \partial u_i/\partial s$. The kernels $\boldsymbol{U}$ and $\boldsymbol{W}$ are given in Appendix B. An equation relating the stress tensor $\boldsymbol{\sigma}$ at a boundary point to $\boldsymbol{\tau}$ and $\boldsymbol{\Delta}$ at that point, can be found, for example, in Zhang and Mukherjee [24].

It is important to restate that the present error estimation method can be used in conjunction with the standard BEM (Eq. (20)), the DBEM (Eq. (21)) or other alternative BEM formulations, such as the Boundary Contour Method (BCM) [25] [26] or Galerkin type methods, e.g. [27]. For reasons given below, the DBEM is adopted in this work.

6.2 Choice of primary variables

In this work, the error indicators are formulated in terms of tractions and displacement derivatives (rather than in terms of tractions and displacements). Reasons for this choice, based on both theoretical as well as practical arguments, are given below.

Theoretical evidence, based on the notion of Error Equidistribution [28], can be found in the literature on adaptive methods. For example, in the FEM, Diaz et al. [29] have presented a method for mesh optimization. The condition for obtaining optimum meshes, in second order elliptic boundary value problems, is expressed in terms of Sobolev seminorms for displacements (see Eqs. (18) and (19) of Diaz et al. [29, page 36]). These seminorms involve displacement derivatives rather than displacements themselves. Analogous arguments, to the ones used by Diaz et al. [29], have been employed by Ingber and Mitra [30] in the solution of biharmonic equations by the BEM.

It is worth quoting two statements from the literature, based on practical experience, which also confirm the point of this Section. The first one is with respect to the FEM, and the second one is with respect to the BEM. Zienkiewicz and Zhu [12, p. 1382] have stated that "... we have concentrated here on error norms involving the derivatives ($\boldsymbol{\sigma}$) and not the basic function $\boldsymbol{u}$ (such as displacements)." Guiggiani and Lombardi [15, p. 272] have stated that "... two displacement fields should be regarded as truly different when they have different gradients, not just because of a different mean value. Different mean values are generally related to errors in other parts of the boundary".

Table 1 summarizes the primary variables in both the BEM and DBEM. Since the DBEM employs tractions and displacement derivatives, it provides an adequate set of primary variables. Therefore, it is the method of choice in the present work.

Table 1. Primary variables for BEM and DBEM ($i = 1, 2$)

Method	Equation	Primary	variables
BEM	20	u_i	τ_i
DBEM	21	$\dfrac{\partial u_i}{\partial s}$	τ_i

6.3 Sensitivity formulation

A DBEM for sensitivities has been presented by Zhang and Mukherjee [24]. By applying the DDA to Eq. (21), they have obtained the following equation for sensitivities:

$$\int_{\partial B} [U_{ij}(\boldsymbol{b}; P, Q)\, \overset{*}{\tau}_i(\boldsymbol{b}; Q) - W_{ij}(\boldsymbol{b}; P, Q)\, \overset{*}{\Delta}_i(\boldsymbol{b}; Q)]\, ds(\boldsymbol{b}; Q)$$

$$+ \int_{\partial B} [\overset{*}{U}_{ij}(\boldsymbol{b}; P, Q)\, \tau_i(\boldsymbol{b}; Q) - \overset{*}{W}_{ij}(\boldsymbol{b}; P, Q)\, \Delta_i(\boldsymbol{b}; Q)]\, ds(\boldsymbol{b}; Q) \tag{22}$$

$$+ \int_{\partial B} [U_{ij}(\boldsymbol{b}; P, Q)\, \tau_i(\boldsymbol{b}; Q) - W_{ij}(\boldsymbol{b}; P, Q)\, \Delta_i(\boldsymbol{b}; Q)]\, \overset{*}{ds}(\boldsymbol{b}; Q) = 0$$

where a superscribed $*$ denotes a derivative with respect to a typical component $b_i \equiv b$ of a design vector $\boldsymbol{b}$, i.e.

$$\overset{*}{(\cdot)} = \frac{\partial}{\partial b}(\cdot). \tag{23}$$

The design variables in this work are defined as coordinates of nodal positions. Calculations of $\overset{*}{ds}$ within the scope of standard sensitivity analysis can be found, for example, in References [24], [31]. The particular choice of the design vector is discussed further in Section 6.4.

From Eqs. (22) and (16), a special sensitivity version of the governing DBEM formulation, for this work, obtained by means of the DDA, is

$$\int_{\partial B} [U_{ij}(\boldsymbol{b}; P, Q)\, \overset{*}{\tau}_i(\boldsymbol{b}; Q) - W_{ij}(\boldsymbol{b}; P, Q)\, \overset{*}{\Delta}_i(\boldsymbol{b}; Q)]\, ds(\boldsymbol{b}; Q)$$

$$+ \int_{\partial B} [\overset{*}{U}_{ij}(\boldsymbol{b}; P, Q)\, \tau_i(\boldsymbol{b}; Q) - \overset{*}{W}_{ij}(\boldsymbol{b}; P, Q)\, \Delta_i(\boldsymbol{b}; Q)]\, ds(\boldsymbol{b}; Q) = 0. \tag{24}$$

It is worth mentioning that the sensitivity formulation, presented in Eq. (24), is different from the one used in shape design sensitivity analysis, where the shape of the body under study changes continuously (see, for example, References [24] and [32]). Here, the shape of the body remains unaltered. Moreover, the design perturbations in this work involve *moving* the middle points of quadratic elements along the boundary elements themselves, so that a differential element ds remains unaffected [4]. Consequently, the extra term associated with $\overset{*}{ds}$ does not contribute to Eq. (24).

It has been shown [24], [31] that

$$\overset{*}{U}_{ij}(\boldsymbol{b}; P, Q) = U_{ij,k}(\boldsymbol{b}; P, Q)\, [\overset{*}{x}_k(Q) - \overset{*}{x}_k(P)] \tag{25}$$

$$\overset{*}{W}_{ij}(\boldsymbol{b}; P, Q) = W_{ij,k}(\boldsymbol{b}; P, Q)\, [\overset{*}{x}_k(Q) - \overset{*}{x}_k(P)] \tag{26}$$

where $\overset{*}{x}$ is the design velocity at a boundary point. Note that both $\overset{*}{\boldsymbol{U}}$ and $\overset{*}{\boldsymbol{W}}$ are regular by virtue of the fact that

$$\overset{*}{x}_k(Q) - \overset{*}{x}_k(P) \sim O(r) \tag{27}$$

where r is the Euclidean distance between P and Q.

Note that geometrical variables (here the positions of the source and field points) appear explicitly in the expressions of the kernels $\boldsymbol{U}$ (Eq. (B.1)) and $\boldsymbol{W}$ (Eq. (B.3)) in Eq. (21). Further, since

in this work the design variables are also geometric, the sensitivity version of the DBEM, Eq. (24), explicitly accounts for the geometry through the design velocities $\overset{*}{x}$ in Eqs. (25) and (26). Also, since the *star* quantities ($\overset{*}{\tau}$, $\overset{*}{\Delta}$; $\overset{*}{U}$, $\overset{*}{W}$) are associated with geometry, Eq. (24) is strongly influenced by geometrical variables.

6.4 Design velocities

The main idea in the proposed error estimation method is the explicit consideration of both geometrical and physical variables of the problem. A procedure, which relies on the consideration of geometrical variables, is presented for obtaining the design velocities (sensitivities of the coordinates of boundary nodes with respect to appropriate design variables) in 2-D BEM problems. This involves parameterization of element curves. Extension of this procedure to 3-D BEM problems involves parameterization of element surfaces. Techniques for representation of curves and surfaces can be found, for example, in the survey paper by Böhm et al. [33].

As mentioned above, design velocities are sensitivities of the coordinates of boundary nodes, here the mid-nodes of quadratic boundary elements, with respect to appropriate design variables. For 2-D problems, a design variable must be chosen such that the direction of the design perturbation of a node is tangential to the boundary ∂B at that point. Thus, use of a parameterization in terms of the arc length s on ∂B is an obvious choice. In 2-D, a boundary element is therefore geometrically parameterized as $x(s) = (x_1(s), x_2(s))$.

With reference to Fig. 4a, a generic internal point B on a boundary element has the coordinates

$$x_i(B) \equiv x_i(s)|_{s=L_0+bL} = x_i(L_0 + bL) \tag{28}$$

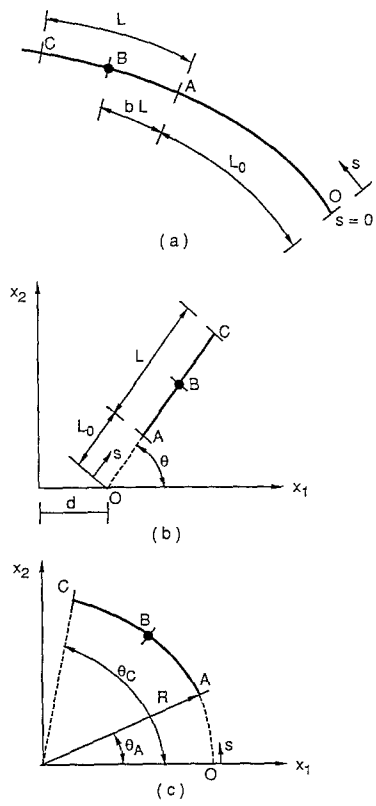

Fig. 4. Boundary elements with parameterization along the arc length; **a** general; **b** straight line; and **c** arc of a circle

where $i = 1, 2$ and $s = L_0 + bL$ at B, with

$$L = \int_A^C ds, \quad L_0 = \int_O^A ds \tag{29}$$

the length of the boundary segment AC and the length of the arc OA, respectively. The reference point O is at $s = 0$.

The only design variable here is the scalar $b \in [0, 1]$ such that bL measures the distance, along the curve, from point A to a generic point B along a boundary element. If B is the middle point of the element, $b = 0.5$. *This choice of parameterization is quite general and also very efficient since the perturbation of a single scalar variable b perturbs all the middle nodes of all the boundary elements on ∂B in a regulated manner*. Note that this particular choice of design variables makes the error estimation method practical for engineering applications.

The present approach consists of deriving analytical expressions for $\overset{*}{x}_i$, $i = 1, 2$, for each type of boundary curve involved in a given problem, e.g. segment of a straight line, arc of a circle, parabola, hyperbola, Hermite, etc. Next, design velocities are calculated for the first two cases. Other shapes can be handled in a similar fashion.

6.4.1 Special case 1 – segment of a straight line

With reference to Fig. 4b,

$$\begin{aligned} x_1(s) &= d + s\cos(\theta), \\ x_2(s) &= s\sin(\theta). \end{aligned} \tag{30}$$

At B,

$$\begin{aligned} x_1(B) &= d + (L_0 + bL)\cos(\theta) = x_1(A) + bL\cos(\theta), \\ x_2(B) &= (L_0 + bL)\sin(\theta) = x_2(A) + bL\sin(\theta), \end{aligned} \tag{31}$$

so that

$$\begin{aligned} \overset{*}{x}_1(B) &= L\cos(\theta), \\ \overset{*}{x}_2(B) &= L\sin(\theta). \end{aligned} \tag{32}$$

6.4.2 Special case 2 – arc of a circle

With reference to Fig. 4c,

$$\begin{aligned} x_1(s) &= R\cos\left(\frac{s}{R}\right), \\ x_2(s) &= R\sin\left(\frac{s}{R}\right). \end{aligned} \tag{33}$$

At B, with $L_0 = R\theta_A$ and $L = R(\theta_C - \theta_A)$,

$$\begin{aligned} x_1(B) &= R\cos[\theta_A + b(\theta_C - \theta_A)], \\ x_2(B) &= R\sin[\theta_A + b(\theta_C - \theta_A)], \end{aligned} \tag{34}$$

so that

$$\begin{aligned} \overset{*}{x}_1(B) &= -R \sin [\theta_A + b(\theta_C - \theta_A)] (\theta_C - \theta_A), \\ \overset{*}{x}_2(B) &= R \cos [\theta_A + b(\theta_C - \theta_A)] (\theta_C - \theta_A). \end{aligned} \tag{35}$$

6.5 Discretization

Equation (21), for tractions and tangential displacement derivatives, and Eq. (24), for sensitivities of both tractions and tangential displacement derivatives, are discretized as follows. The boundary is subdivided into piecewise quadratic conforming boundary elements where the variables τ_i, Δ_i in Eq. (21), and $\overset{*}{\tau}_i$, $\overset{*}{\Delta}_i$ in Eq. (24) are approximated. The logarithmically singular kernels are treated using log-weighted integration (see, for example, Appendix A of [34]).

Due to the adopted Eulerian approach for sensitivity calculations (see Section 5), the numerical discretization of Eq. (24) deserves special attention. Recall Eq. (19) and let the response variable now be τ or Δ, instead of ϕ. Therefore, for each boundary element

$$\overset{*}{\tau}(\xi) = \overset{*}{\tau}_A M_1(\xi) + \overset{*}{\tau}_B M_2(\xi) + \overset{*}{\tau}_C M_3(\xi) + \underline{\frac{1}{2} (\tau_A - \tau_C) M_2(\xi)}, \tag{36}$$

$$\overset{*}{\Delta}(\xi) = \overset{*}{\Delta}_A M_1(\xi) + \overset{*}{\Delta}_B M_2(\xi) + \overset{*}{\Delta}_C M_3(\xi) + \underline{\frac{1}{2} (\Delta_A - \Delta_C) M_2(\xi)}. \tag{37}$$

Note that, in addition to the usual terms in a quadratic interpolation, there is an extra term (underlined) in Eqs. (36) and (37). When solving for the sensitivities $(\overset{*}{\tau}, \overset{*}{\Delta})$, the contributions involving these terms are known and can be taken to the RHS of the system of equations.

After the collocation[3] and assembling processes are completed, the resulting systems associated with Eqs. (21) and (24) are of the form

$$\begin{aligned} [A] \{\tau\} + [B] \{\Delta\} &= \{0\}, \\ [A] \{\overset{*}{\tau}\} + [B] \{\overset{*}{\Delta}\} &= \{h\}, \end{aligned} \tag{38}$$

respectively, where the standard and sensitivity systems of equations share the same governing discrete operators $[A]$ and $[B]$, and $\{h\}$ is a known vector. After switching appropriate columns, one obtains

$$\begin{aligned} [K] \{x\} &= \{c_1\}, \\ [K] \{\overset{*}{x}\} &= \{c_2\} \end{aligned} \tag{39}$$

for the boundary unknowns $\{x\}$ and $\{\overset{*}{x}\}$. It is important to observe that Eqs. (39) are governed by the same discrete operator $[K]$. Moreover, the vector $\{c_2\}$ contains the contributions from both the first and second lines of Eq. (24) because of the reasons explained above, with respect to Eqs. (36) and (37). Finally, Eqs. (38) and (39) are overdetermined but have full column rank [24]. Here they have been solved by QR decomposition [35].

6.6 Error indicators

Some heuristic arguments are used to propose the form of the error indicators. The basic ideas for deriving the error indicators in this work are simplicity and completeness. In the interest of

[3] Here "collocation" means to enforce the respective BIE at a series of selected points which are element nodal points.

simplicity, discrete quantities are used here. However, integrated quantities can also be used (e.g. Guiggiani [14]). What is meant by completeness is that all the primary variables in the problem must be explicitly included in the error indicator scheme.

From the boundary integral equation for sensitivities, Eq. (24), there are four primary boundary variables at each boundary point. These variables are: $\overset{*}{\tau}_i$, $\overset{*}{\Delta}_i$, $i = 1, 2$. Typically, either $\overset{*}{\tau}_1$ or $\overset{*}{\Delta}_1$, and either $\overset{*}{\tau}_2$ or $\overset{*}{\Delta}_2$, are prescribed, while the rest is unknown. An error indicator at an element, $\eta^{(e)}$, is defined as follows. First, consider the normalized nodal sensitivities

$$\begin{aligned} \bar{\overset{*}{\tau}}_n^{(e)} &= \frac{w_\tau^{*(e)} \overset{*}{\tau}_n^{(e)}}{\overset{*}{\tau}_{\text{ref}}}, \qquad \bar{\overset{*}{\tau}}_t^{(e)} = \frac{w_\tau^{*(e)} \overset{*}{\tau}_t^{(e)}}{\overset{*}{\tau}_{\text{ref}}} \\ \bar{\overset{*}{\Delta}}_n^{(e)} &= \frac{w_\Delta^{*(e)} \overset{*}{\Delta}_n^{(e)}}{\overset{*}{\Delta}_{\text{ref}}}, \qquad \bar{\overset{*}{\Delta}}_t^{(e)} = \frac{w_\Delta^{*(e)} \overset{*}{\Delta}_t^{(e)}}{\overset{*}{\Delta}_{\text{ref}}} \end{aligned} \tag{40}$$

where

$$\begin{aligned} \overset{*}{\tau}_{\text{ref}} &= \sqrt{\sum_{e=1}^{N} (w_\tau^{*(e)})^2 \left[(\overset{*}{\tau}_n^{(e)})^2 + (\overset{*}{\tau}_t^{(e)})^2 \right]} \\ \overset{*}{\Delta}_{\text{ref}} &= \sqrt{\sum_{e=1}^{N} (w_\Delta^{*(e)})^2 \left[(\overset{*}{\Delta}_n^{(e)2} + (\overset{*}{\Delta}_t^{(e)})^2 \right]} . \end{aligned} \tag{41}$$

Here, N is the total number of boundary elements, and the subscripts n and t refer to the normal and tangential components, respectively, of the relevant boundary quantities.

The functions $w_\tau^{*(e)}$ and $w_\Delta^{*(e)}$ refer to weighting parameters for the sensitivities of tractions and tangential displacement derivatives, respectively. In this work,

$$w_\tau^{*(e)} = w_\Delta^{*(e)} = w^{(e)} \tag{42}$$

is found to be adequate. *Note that, physically, both primary variables, i.e. tractions and displacement derivatives (see Eq. (21)), are of similar nature because both are functions of first order displacement derivatives.* Therefore, the function $w^{(e)}$ refers to the weighting for the element. This type of parameter may be chosen based on the notion of error equidistribution (see Section 6.2). For example, typical weight parameters are

$$w^{(e)} = 1, \qquad w^{(e)} = f(L^{(e)})$$

where $f(L^{(e)})$ denotes a function of the element length $L^{(e)}$ (normalized). For the sake of simplicity, $w^{(e)} = 1$ is adopted in the present work. As mentioned before, the sensitivities are evaluated at the mid-points of each boundary element.

Finally, the error indicator at an element is:

$$\eta^{(e)} = \max \left[|\bar{\overset{*}{\tau}}_n^{(e)}|, \quad |\bar{\overset{*}{\tau}}_t^{(e)}|, \quad |\bar{\overset{*}{\Delta}}_n^{(e)}|, \quad |\bar{\overset{*}{\Delta}}_t^{(e)}| \right]. \tag{43}$$

7 Computational results

Two examples of plane strain problems in linear elasticity, for which analytical solutions are available, are considered in this Section. The first one is a circular cylinder with a concentric cylindrical hole under internal pressure. The second one is a finite portion of an infinite plate, with a centered circular hole, subjected to remote uniaxial tension. *For each example, each*

segment of the boundary is subdivided into uniform boundary elements. This is done so as not to bias the mesh *a priori* to reflect the nature of the solution. Standard isoparametric quadratic boundary elements are used for representation of both the geometry and the boundary variables τ, Δ, $\overset{*}{\tau}$ and $\overset{*}{\Delta}$ (see Zhang and Mukherjee [24] for details regarding discretization and modeling of corners).

The error indicator $\eta^{(e)}$ is computed at each element mid-point according to Eqs. (40) to (43). In Section 4, it has been conjectured that the nodal sensitivity of the response function is related to the slope of the error. Thus these nodal sensitivities are taken as the error indicators $\eta^{(e)}$, Eq. (43), which can be readily used as drivers for adaptive meshing. The idea, in the numerical examples presented below, is to calculate the error indicators $\eta^{(e)}$ and to carry out some evaluation of their performance.

7.1 Circular cylinder under internal pressure

Figure 5a shows a hollow cylinder, under internal pressure, in plane strain. The inner and outer radii of the cylinder are $a = 1.0$ and $b = 1.5$, respectively. The material constants are $G = 5880.0$ and $\nu = 0.3$. The applied internal pressure is $p = 12$. Consistent units are used. The boundary conditions on a quarter of the cylinder are shown in Fig. 5b. The boundary of the quarter cylinder is discretized with 5 uniform quadratic elements on each segment – with a total of 20 elements.

The analytical solution for stresses (Lamé's solution, first published in 1833) and displacements for a thick-walled circular cylinder under internal pressure can be found, for example, in the book by Cook and Young [36, pp. 91–92]. If desired, this solution can be used to calculate the actual local errors (see Eq. (1)).

The numerical results obtained are summarized in Table 2. The dominant quantities and the range of the error indicator $\eta^{(e)}$ on each segment (see Fig. 5b) are obtained according to Eq. (43). Note that, in order to show the scaling effect of the reference quantities (see Eqs. (40) and (41)), the maximum value of $\eta^{(e)}$ (i.e. 0.6 in the last column of Table 2) is not renormalized to the unit.

Further examination of this example reveals certain important facts. It is seen that the error indicators on the segments AB and CD are nearly symmetric, as expected, with larger values near the high stress concentration points A and D. Thus, this distribution of $\eta^{(e)}$ would suggest subdivision of elements near point A in segment AB and point D in segment CD, in an adaptive scheme. Also, $\eta^{(e)}$ is low on the segment BC as expected, since the far field stress gradients are

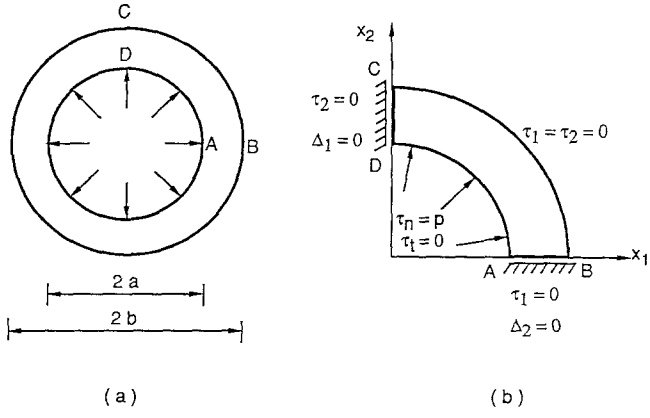

Fig. 5. Example 1 – Hollow cylinder under internal pressure; **a** configuration; **b** boundary conditions

Table 2. Error indicators around the quarter cylinder with $b/a = 1.5$ (see Fig. 5)

Segment	Elements	Dominant quantities	Range of $\eta^{(e)}$
AB	1–5	τ_n	0.6–0.05
BC	6–10	Δ_n	≈ 0.05
CD	11–15	τ_n	0.05–0.6
DA	16–20	Δ_n	≈ 0.45

Table 3. Error indicators around the quarter cylinder with $b/a = 4.0$ and $\alpha = 1.146$ (see Fig. 5)

Segment	Elements	Dominant quantities	Range of $\eta^{(e)}$
AB	1–5	τ_n	0.7–0.01
BC	6–8	Δ_n	≈ 0.01
CD	9–13	τ_n	0.01–0.7
DA	14–16	Δ_n	≈ 0.57

small in this example. The situation on segment DA is particularly interesting. In this axisymmetric problem, the tangential gradients of quantities of interest are zero along DA. This might suggest that only a few elements (to model the geometry) are sufficient on DA. It is important to note, however, that radial stress gradients are significant along DA, and intuitively one expects that a fine mesh should be used wherever the magnitude of the gradient vector of a solution field is high. The error indicators reflect the physics of the problem by virtue of the fact that $\eta^{(e)}$ contains geometrical information regarding curvature of segment DA. Qualitatively, this fact is obvious from Figs. 10 b and 11 b of Zienkiewicz and Zhu [10] which show optimized domain meshes, for the FEM, applied to the same type of problem. In view of the above, the error indicator being uniform and reasonably high on segment DA (see Table 2) is particularly encouraging.

In summary, all the features of $\eta^{(e)}$ in Table 2 appear to be consistent in this example. It should be repeated here that the mesh used in this example is piecewise uniform on the four boundary segments, and therefore unbiased with respect to the expected solution for this problem.

Next, the above problem was attempted with the same mesh (5 uniform quadratic elements on each segment) but for $a = 1.0$ and $b = 4.0$ according to the notation of Fig. 5 a. Not surprisingly, it was realized from this example that the ratio (see Fig. 5)

$$\alpha = \frac{\text{Element length on } AB}{\text{Element length on } DA}$$

is an important factor. For the case $b/a = 3$, $\alpha = 1.273$, while for $b/a = 4.0$, $\alpha = 1.91$, if a fixed number of uniform elements is used on each of the segments AB and DA. In view of this, the discretization for the case $b/a = 4.0$ was changed to 5 uniform elements on each of the segments AB and CD, and 3 uniform elements on each of the segments DA and CB. For this case, $\alpha = 1.146$. It should be mentioned here that the discretization on the segment BC is relatively unimportant since the stress gradients are small there. Numerical results for the error indicators, for the case $b/a = 4$ and $\alpha = 1.146$, are excellent. These are shown in Table 3.

7.2 A plate with a circular hole under remote uniaxial tension

Figure 6a shows an infinite plate, with a centered circular hole, subjected to remote uniaxial tension. Figure 6b shows the portion of the plate to be analyzed assuming plane strain state. The boundary conditions on the quarter plate, obtained from the mechanics fields for the infinite plate (see Fig. 6a), are shown in Fig. 6c. The size of the full plate is 100×100 and the hole diameter is 10.0. The material constants are $E = 5880.0$ and $\nu = 0.3$. The applied remote tension is $\sigma_\infty = 1.0$. Consistent units are used here. The boundary of the quarter plate is discretized with 5 uniform quadratic elements on each segment (as in the previous example) — with a total of 25 elements.

The complete analytical solution for stresses (first obtained by G. Kirsch in 1898) and displacements for the present example can be found in the classical book by Muskhelishvili [37, p. 205]. If desired, this solution can be used to calculate the actual local errors (see Eq. (1)).

The error indicator $\eta^{(e)}$ as a function of element number is shown in Fig. 7. The dominant quantities on each segment, according to Eq. (43), are also given in the caption of this figure. Again, these are the error indicators evaluated at the mid-point of the elements. Careful examination of Fig. 7, as in the previous example, reveals correct trends. The error indicator distributions on the segments AB and DE have opposite trends, as expected. The indicator is high near the stress concentration point A and low on the far field segments BC and CD. Finally, the distribution of $\eta^{(e)}$ on the circular boundary EA has progressively larger values as one moves from point E to point A. In an adaptive scheme, this suggests the use of small elements near point A (with a stress concentration of 3 for the infinite plate) and relatively larger ones near point E where the tangential stress is compressive but of magnitude equal to that of the remote tensile stress σ_∞.

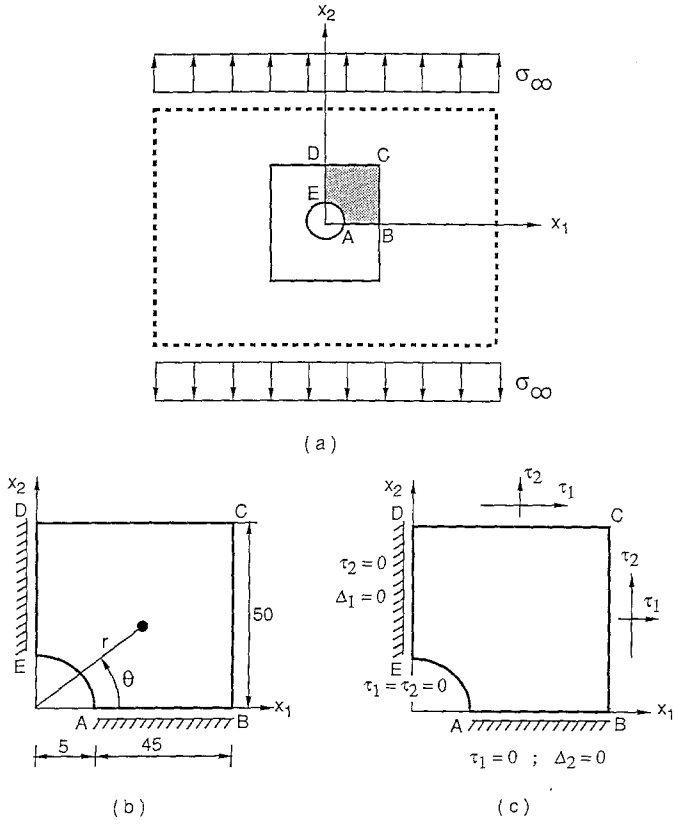

Fig. 6. Example 2 — **a** Infinite plate, with a centered circular hole, subjected to uniaxial tension; **b** portion of the plate analyzed here; **c** boundary conditions

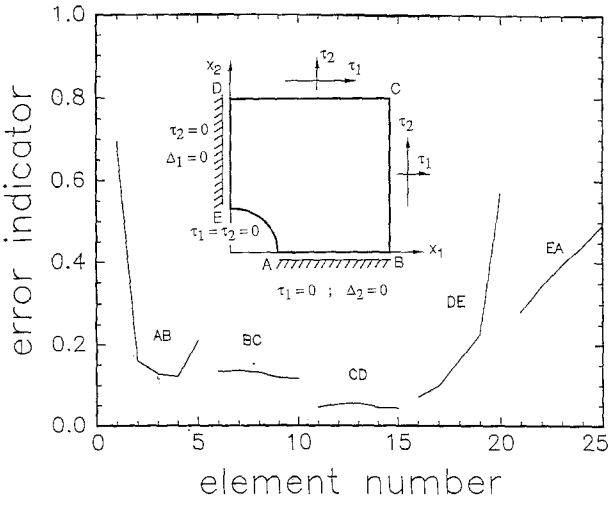

Fig. 7. Example 2 – Error indicator $\eta^{(e)}$ around the quarter plate. The dominant quantities on each segment are: AB: τ_n; BC: Δ_n; CD: Δ_n, Δ_t; DE: τ_n; EA: Δ_n

Relatively poor numerical accuracy of the DBEM, with this *coarse piecewise uniform mesh*, results for the calculation of Δ over EA, in this particular example. It is encouraging to note that even though there are substantial errors in the numerical results for Δ over the circular boundary EA, the error indicator $\eta^{(e)}$, nevertheless, shows the correct behaviour over this segment. This fact is a tribute to the robustness of $\eta^{(e)}$ as an error indicator, at least for this example. Further details about this example can be found in Ref. [4]. It should be mentioned here that with a more "realistic" mesh the DBEM gives excellent results for this type of problem, as shown by Ghosh et al. [22].

8 Conclusions and extensions

This paper proposes the idea using nodal sensitivities as error estimates in computational mechanics calculations. Their performance as error indicators is evaluated in two numerical examples. These sensitivities appear to provide a good indication of the error in uniformly coarse grid approximations. The advantages of the new error estimation method presented herein are: (1) computationally efficient scheme; (2) explicit consideration of both geometrical and physical variables; (3) natural linkage between geometric modeling and numerical analysis; and (4) generality (applicable to boundary-type formulations, e.g. BEM, as well as domain-type formulations, e.g., FEM, and to various operators, e.g., harmonic, biharmonic, etc.). This last advantage might prove useful for error estimation when coupled numerical methods are used, e.g. BEM and FEM [38].

In the present work, the error estimation method has been developed in conjunction with the BEM (see Section 6). Use of the new method in conjunction with the FEM requires sensitivity analysis of the governing equations [39], [40]. The process for obtaining nodal sensitivities, by the DDA, involves direct analytical differentiation of the element stiffness matrices. An efficient numerical technique for differentiating the element stiffness matrix, which can be readily applied here, has been presented by Lin and Abel [41].

Comments on the nodal perturbation scheme, for calculations of nodal sensitivities in the 3-D BEM, as well as both the 2-D and 3-D FEM, are in order. For consistency, this explanation is given here with regard to quadratic elements. For the 3-D BEM and 2-D FEM, the nodal perturbation schemes are similar. In this case, two design variables are needed. The midside nodes of eight-node quadratic (Q8 family) elements, for example, are perturbed along the element edges. This scheme has the advantage of being general, i.e. it can be applied to corner elements as well as interior elements. The nodal perturbations on the curved surface of a body must lie on the local tangent plane, in specific chosen directions. The idea of surface gradients and directional derivatives on the local tangent plane (see, for example, Bonnet and Bui [42]), might prove to be useful for this purpose. Further information on surface geometry can be found in the book by Sokolnikoff [43]. For the 3-D FEM, nodal perturbations involve nodes on the surface as well as nodes in the interior. In this case, 3 design variables are needed. The midside nodes of twenty-node brick (B20) elements, for example, should be perturbed. Perturbation of nodes on the surface is analogous to the 3-D BEM case, explained previously. Perturbations of interior nodes are in the directions of the global frame of reference.

It is worth mentioning that, in this work, nodal perturbations have been discussed in the context of quadratic elements. However, in principle, the method presented here can also be extended to linear or higher order elements [4].

We feel that the new error estimation method presented here deserves further attention. An immediate subject of future work is the investigation of the proposed error indicators in a self-adaptive analysis. Possible adaptive strategies include h-remeshing (increasing mesh refinement), p-enrichment (increasing degree of polynomial shape functions), r-relocation (relocation of the nodes of a grid with fixed topology in order to satisfy a set of optimality conditions), and combined methods (e. g. $r-h, r-h-p$). It is also worth investigating alternative forms of the error indicator (other than the one in Eq. (43)), such as one which still uses sensitivity quantities, but is free from scaling effects of reference quantities (see Eqs. (40) and (41)) and has an intrinsic physical meaning (such as energy) attached to it.

The range of application of the idea of using nodal sensitivities as errors is large, even though, in this paper, we have concentrated on linear elasticity problems by the BEM. However, it is clear that use of nodal sensitivities as error estimates has potential advantages in many fields of computational mechanics.

Appendix A: generalized proof of Eq. (11): $\overset{*}{\phi}_{ea} = e_{\phi}'$

A shorter and more general proof of Eq. (11) follows. The overall procedure is illustrated by Fig. 8, which is a modified version of Fig. 2. Let $\phi_a(\xi)$ be a quadratic interpolation of $\phi_e(\xi)$ with the interior interpolation point located at $\xi = \xi_0$. Thus

$$\phi_a(\xi_0) = \phi_e(\xi_0). \tag{A.1}$$

Let $\phi_{ea}(\xi)$ be a quadratic interpolation of $\phi_e(\xi)$ with the interior interpolation point located at $\xi = \xi_0 + \varepsilon$. Therefore,

$$\phi_{ea}(\xi_0 + \varepsilon) = \phi_e(\xi_0 + \varepsilon). \tag{A.2}$$

Since the interpolation is quadratic, exact Taylor expansion gives

$$\phi_a(\xi_0 + \varepsilon) = \phi_a(\xi_0) + \frac{d\phi_a(\xi_0)}{d\xi}\varepsilon + \frac{1}{2}\frac{d^2\phi_a(\xi_0)}{d\xi^2}\varepsilon^2. \tag{A.3}$$

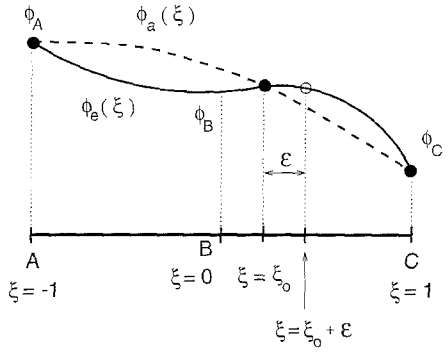

Fig. 8. Quadratic interpolation of $\phi_e(\xi)$ considering a generic interior point

Thus,

$$\phi_{ea}(\xi_0 + \varepsilon) - \phi_a(\xi_0 + \varepsilon) = \phi_{ea}(\xi_0 + \varepsilon) - \phi_a(\xi_0) - \frac{d\phi_a(\xi_0)}{d\xi}\varepsilon - \frac{1}{2}\frac{d^2\phi_a(\xi_0)}{d\xi^2}\varepsilon^2 \tag{A.4}$$

and substitution of Eqs. (A.1) and (A.2) into Eq. (A.4) yields

$$\phi_{ea}(\xi_0 + \varepsilon) - \phi_a(\xi_0 + \varepsilon) = \phi_e(\xi_0 + \varepsilon) - \phi_e(\xi_0) - \frac{d\phi_a(\xi_0)}{d\xi}\varepsilon - \frac{1}{2}\frac{d^2\phi_a(\xi_0)}{d\xi^2}\varepsilon^2. \tag{A.5}$$

Dividing this equation by ε and taking the limit as $\varepsilon \to 0$, one obtains

$$\lim_{\varepsilon\to 0}\left[\frac{\phi_{ea}(\xi_0 + \varepsilon) - \phi_a(\xi_0 + \varepsilon)}{\varepsilon}\right] = \lim_{\varepsilon\to 0}\left[\frac{\phi_e(\xi_0 + \varepsilon) - \phi_e(\xi_0)}{\varepsilon}\right] - \frac{d\phi_a(\xi_0)}{d\xi}. \tag{A.6}$$

Note that the limit term on the left-hand-side is $\overset{*}{\phi}_{ea}(\xi_0, 0)$ and the limit term on the RHS is $d\phi_e(\xi_0)/d\xi$. Therefore, the RHS of Eq. (A.6) is $d[\phi_e(\xi_0) - \phi_a(\xi_0)]/d\xi = de_\phi(\xi_0)/d\xi = e_\phi'(\xi_0)$, and thus

$$\overset{*}{\phi}_{ea}(\xi_0, 0) = e_\phi'(\xi_0). \tag{A.7}$$

Equation (A.7) is a generalized proof of Eq. (11) because ξ_0 does not need to be located at the middle point ($\xi = 0$) of the element.

Appendix B: BEM and DBEM kernels

The BEM and DBEM kernels for 2-D problems are presented here. The BEM kernels (see Eq. (20)) are obtained from Kelvin's singular solutions for a point force in a mathematically infinite elastic body. These kernels are available in many references on the BEM, e.g., Rizzo [19]. They are

$$U_{ij} = \frac{1}{8\pi(1-\nu)G}\left[(3 - 4\nu)\ln\frac{1}{r}\delta_{ij} + r_{,i}r_{,j}\right], \tag{B.1}$$

$$T_{ij} = -\frac{1}{4\pi(1-\nu)r}\left\{\frac{\partial r}{\partial \boldsymbol{n}}[(1 - 2\nu)\delta_{ij} + 2r_{,i}r_{,j}] + (1 - 2\nu)(n_j r_i - n_i r_j)\right\} \tag{B.2}$$

where δ_{ij} is Kronecker delta, G is the shear modulus and ν is Poisson's ratio of the material. Also, r is the Euclidean distance between a source point P (or p) and a field point Q (or q). The

upper case letters P and Q denote points on the boundary ∂B while the lower case letters p and q denote points in B. A comma denotes a derivative with respect to the corresponding coordinate of the field point. Finally, $\boldsymbol{n}$ denotes the unit outward normal to ∂B, and $\partial r/\partial \boldsymbol{n}$ is the derivative of r with respect to the normal at a field point.

The DBEM kernels [22] are $\boldsymbol{U}$, as given by the previous Eq. (B.1), and $\boldsymbol{W}$, given below

$$W_{ij} = \frac{1}{4\pi(1-\nu)} [2(1-\nu)\,\psi\delta_{ij} + \gamma_{ik} r_{,j} r_{,k} - (1-\nu)\,\gamma_{ij} \ln r] \tag{B.3}$$

where

$$\gamma_{11} = \gamma_{22} = 0, \quad \gamma_{12} = -\gamma_{21} = 1$$

and ψ is the angle, measured in a counter-clockwise sense, between the line joining P and Q (i.e. $r(P, Q)$) and a reference direction, e.g., the line through P parallel to the global x_1 axis (see, for example, Fig. 1 in Ghosh et. al. [22, p. 70]).

Acknowledgements

G. H. Paulino acknowledges partial financial support provided by CNPq ('Conselho Nacional de Desenvolvimento Científico e Tecnológico'), the Brazilian agency for research and development. F. Shi acknowledges the financial support from Xerox Corporation through the Design Research Institute at Cornell University. S. Mukherjee acknowledges the financial support of the National Science Foundation through grant number MSS-9301443 to Cornell University. The authors are grateful to Prof. M. Guiggaini of the "Universitá degli Studi di Pisa" (Italy), for his comments on this work. The first author acknowledges very useful discussions with Dr. P.-C. Huang and Dr. P. A. Wawrzynek.

References

[1] Tworzydlo, W. W., Oden, J. T.: Towards an automated environment in computational mechanics. Comput. Methods Appl. Mech. Eng. **104,** 87–143 (1993).
[2] Finnigan, P. M., Kela, A., Davis, J. E.: Geometry as a basis for finite element automation. Eng. Comput. **5,** 147–160 (1989).
[3] Shephard, M. S., Finnigan, P. M.: Integration of geometric modeling and advanced finite element preprocessing. Finite Elem. Anal. Des. **4,** 147–162 (1988).
[4] Paulino, G. H.: Novel formulations of the boundary element method for fracture mechanics and error estimation. Ph.D. dissertation, Cornell University, Ithaca, New York, U.S.A., 1995.
[5] Kelly, D. W., Mills, R. J., Reizes, J. A., Miller, A. D.: A posteriori estimates of the solution error caused by discretization in the finite element, finite difference and boundary element methods. Int. J. Numer. Methods Eng. **24,** 1921–1939 (1987).
[6] Mitra, A. K., Salazar, L. R., Sawyer, M. L.: Spline assisted grid optimization scheme for the boundary element method. In: Boundary element XV, Vol. 1 (Brebbia, C. A., Rencis, J. J., eds.), pp. 643–656. Southampton and London: Computational Mechanics Publications and Elsevier Applied Science 1993.
[7] Lean, M. H.: Adaptively meshed boundary integral equation method for nonlinear magnetostatics. IEEE Trans. Magnetics **26,** 614–617 (1990).
[8] Paulino, G. H., Gray, L. J., Zarikian, V.: Hypersingular residuals – A new approach for error estimation in the boundary element method. Int. J. Numer. Methods Eng. **39,** 2005–2029 (1996).
[9] Bugeda, G., Oliver, J.: A general methodology for structural shape optimazition problems using automatic adaptive remeshing. Int. J. Numer. Methods Eng. **36,** 3161–3185 (1993).
[10] Zienkiewicz, O. C., Zhu, J. Z.: A simple error estimator and adaptive procedure for practical engineering analysis. Int. J. Numer. Methods Eng. **24,** 337–357 (1987).

[11] Zienkiewicz, O. C., Zhu, J. Z.: The superconvergent patch recovery and a posteriori error estimates. Part 1: the recovery technique. Int. J. Numer. Methods Eng. **33,** 1331–1364 (1992).
[12] Zienkiewicz, O. C., Zhu, J. Z.: The superconvergent patch recovery and a posteriori error estimates. Part 2: error estimates and adaptivity. Int. J. Numer. Methods Eng. **33,** 1365–1382 (1992).
[13] Sussman, T., Bathe, K.-J.: The gradient of the finite element variational indicator with respect to nodal point coordinates: an explicit calculation and application in fracture mechanics and mesh optimization. Int. J. Numer. Methods Eng. **21,** 763–774 (1985).
[14] Guiggiani, M.: Error indicators for adaptive mesh refinement in the boundary element method – a new approach. Int. J. Numer. Methods Eng. **29,** 1247–1269 (1990).
[15] Guiggiani, M., Lombardi, F.: Self-adaptive boundary elements with *h*-hierarchical shape functions. Adv. Eng. Software **15,** 269–277 (1992).
[16] Henneberger, G., Meunier, G., Sabonnadière, J. C., Sattler, Ph. K., Shen, D.: Sensitivity analysis of the nodal position in the adaptive refinement of finite element meshes. IEEE Trans. Magnetics **26,** 787–790 (1990).
[17] Haftka, R. T., Gürdal, Z.: Elements of structural optimization, 3rd ed. Dordrecht: Kluwer 1992.
[18] Shi, F., Ramesh, P., Mukherjee, S.: Adaptive mesh refinement of the boundary element method for potential problems by using mesh sensitivities as error indicators. Comput. Mech. **16,** 379–395 (1995).
[19] Rizzo, F. J.: An integral equation approach to boundary value problems of classical elastostatics. Q. Appl. Math. **25,** 83–95 (1967).
[20] Guiggiani, M.: The evaluation of Cauchy principal value integrals in the boundary element method – A review. Math. Comput. Model. **15,** 175–184 (1991).
[21] Lutz, E. D., Gray, L. J.: Exact evaluation of singular boundary integrals without CPV. Commun. Numer. Methods Eng. **9,** 909–915 (1993).
[22] Ghosh, N., Rajiyah, H., Ghosh, S., Mukherjee, S.: A new boundary element method formulation for linear elasticity. J. Appl. Mech. Trans. ASME **53,** 69–76 (1986).
[23] Ghosh, N., Mukherjee, S.: A new boundary element method formulation for three-dimensional problems in linear elasticity. Acta Mech. **67,** 107–119 (1987).
[24] Zhang, Q., Mukherjee, S.: Design sensitivity coefficients for linear elastic bodies with zones and corners by the derivative boundary element. Int. J. Solids Struct. **27,** 983–998 (1991).
[25] Nagarajan, A., Lutz, E., Mukherjee, S.: A novel boundary element for linear elasticity with no numerical integration for two-dimensional and line integrals for three-dimensional problems. J. Appl. Mech. Trans. ASME **61,** 264–269 (1994).
[26] Nagarajan, A., Mukherjee, S., Lutz, E.: The boundary contour method for three-dimensional linear elasticity. J. Appl. Mech. Trans. ASME **63,** 278–286 (1996).
[27] Sirtori, S., Maier, G., Novati, G., Miccoli, S.: A Galerkin symmetric boundary-element method in elasticity: formulation and implementation. Int. J. Numer. Methods Eng. **35,** 255–282 (1992).
[28] Oden, J. T., Demkowicz, L.: Advances in adaptive improvements – A survey of adaptive finite element methods in computational mechanics. In: State-of-the-art surveys on computational mechanics (Noor, A. K., Oden, J. T., eds.), pp. 441–467. New York: ASME 1989.
[29] Diaz, A. R., Kikuchi, N., Taylor, J. E.: A method of grid optimization for finite element methods. Comput. Methods Appl. Mech. Eng. **41,** 29–45 (1983).
[30] Ingber, M. S., Mitra, A. K.: Grid optimization for the boundary element method. Int. J. Numer. Methods Eng. **23,** 2121–2136 (1986).
[31] Barone, M. R., Yang, R.-J.: Boundary integral equations for recovery of design sensitivities in shape optimization. AIAA J. **26,** 589–594 (1988).
[32] Zhang, Q., Mukherjee, S., Chandra, A.: Shape design sensitivity analysis for geometrically and materially nonlinear problems by the boundary element method. Int. J. Solids Struct. **29,** 2503–2525 (1992).
[33] Böhm, W., Farin, G., Kahmann, J.: A survey of curve and surface methods in CAGD. Comput. Aided Geom. Des. **1,** 1–60 (1984).
[34] Brebbia, C. A., Telles, J. C. F., Wrobel, L. C.: Boundary element techniques. Berlin, Heidelberg, New York: Springer 1984.
[35] Golub, G. H., Van Loan, C. F.: Matrix computations, 2nd ed. Baltimore, London: The Johns Hopkins University Press 1989.
[36] Cook, R. D., Young, W. C.: Advanced mechanics of materials. New York: Macmillan 1985.
[37] Muskhelishvili, N. I.: Some basic problems of the mathematical theory of elasticity, 4th ed. Groningen – The Netherlands: P. Noordhoff, 1963.

[38] Sirtori, S., Miccoli, S., Korach, E.: Symmetric coupling of finite elements and boundary elements. In: Advances in boundary element techniques (Kane, J. H., Maier, G., Tosaka, N., Atluri, S. N., eds.), pp. 407–427. Berlin, Heidelberg, New York, Tokyo: Springer 1993.
[39] Haug, E. J., Choi, K. K., Komkov, V.: Design sensitivity analysis of structural systems. Orlando: Academic Press 1986.
[40] Arora, J. S., Cardoso, J. B.: Variational principle for shape design sensitivity analysis. AIAA J. **30,** 538–547 (1992).
[41] Lin, S.-C., Abel, J. F.: Variational approach for a new direct-integration form of the virtual crack extension method. Int. J. Fract. **38,** 217–235 (1988).
[42] Bonnet, M., Bui, H. D.: Regularization of the displacement and traction bie for 3d elastodynamics using indirect methods. In: Advances in boundary element techniques (Kane, J. H., Maier, G., Tosaka, N., Atluri, S. N., eds.), pp. 1–29. Berlin, Heidelberg, New York, Tokyo: Springer 1993.
[43] Sokolnikoff, I. S.: Tensor analysis theory and applications to geometry and mechanics of continua. New York: Wiley 1964.

Authors' addresses: G. H. Paulino, School of Civil and Environmental Engineering, Hollister Hall, Cornell University, Ithaca, N. Y., 14853, U. S. A.; Professor S. Mukherjee and F. Shi, Department of Theoretical and Applied Mechanics, Kimball Hall, Cornell University, Ithaca, N. Y., 14853, U.S.A.; P. S. Ramesh, Joseph C. Wilson Center for Research and Technology, Xerox Corporation, 800 Phillips Road, Webster, N.Y. 14580, U.S.A.